Hindawi
Advances in Materials Science and Engineering
Volume 2023, Article ID 3588202, 10 pages
https://doi.org/10.1155/2023/3588202

Research Article

Experimental Investigations of Nano Finishing Process on Nickel-Free Austenitic Stainless Steel by Grey Relational and Principal Component Analysis

S. Kathiresan,[1] G. Anbuchezhiyan,[2] S. Karthikeyan,[3] and Kumaran Palani[4]

[1]*Department of Mechanical Engineering, Prince Shri Venkateshwara Padmavathy Engineering College, Chennai 600127, India*
[2]*Department of Mechanical Engineering, Saveetha School of Engineering, Saveetha Institute of Medical and Technical Sciences, Chennai 602105, Tamil Nadu, India*
[3]*Department of Mechanical Engineering, CEG Campus, Anna University, Chennai 600025, Tamil Nadu, India*
[4]*Department of Mechanical Engineering, College of Engineering, Wolaita Sodo University, Wolaita Sodo, P.O. Box 138, Ethiopia*

Correspondence should be addressed to G. Anbuchezhiyan; tsgaaa1981@gmail.com and Kumaran Palani; pkumaran2003et@gmail.com

Received 19 July 2022; Revised 10 January 2023; Accepted 20 January 2023; Published 24 May 2023

Academic Editor: Dhanesh G. Mohan

The nano surface roughness of metallic materials is important in engineering and medical fields for specific applications. Magneto rheological abrasive flow finishing (MRAFF) process was performed on nickel-free austenitic stainless workpieces in order to obtain surface roughness at the nano level and also to forecast the performance of the MRAFF process in terms of responses such as surface roughness (SR) and material removal rate (MRR). These two responses are affected by process factors such as hydraulic pressure, current to the electromagnet, and the number of cycles performed during the machining process. The design of experiments (DOE) was used to determine the contributions of process parameters to output responses. The techniques of grey relational analysis (GRA) and principal component analysis (PCA) were used in these experimental investigations to discover the process factors that minimise the final Ra and maximise MRR. Through the DOE, a minimum SR of 63.24 nm and a maximum MRR of 2.34 mg/sec were obtained on the samples for the combination of 30 bar pressure, 6 A current, and 300 number of cycles.

1. Introduction

Components with close tolerances and good surface qualities have been created in response to the recent increase in demand for components that fulfill technical and functional criteria for both engineering and medical applications. In general, the micro/nano scale surface roughness of a material has a substantial influence on how well it works in terms of fatigue strength, resistance to wear as well as corrosion, and other associated properties [1].

If the material is a biomaterial such as AISI stainless steel 316L, the surface finish has a strong and precise influence on biocompatibility characteristics such as viability and proliferation of cells followed by adsorption of protein and adhesion of bacteria. The characteristics of biocompatibility, such as cytotoxicity (cell viability and cell proliferation), hemocompatibility, water contact angle, and bio-corrosion, also depend strongly and precisely on the surface finish of the material.

Among the different kinds of austenitic steels, AISI 316L is a common material for orthopaedic, cardiovascular, and orthodontic implants, because of its satisfactory biocompatibility, corrosion resistance, and also viability in cost [2–4]. However, issues have been found with the materials being used in the biomedical field. The most essential issue is the release of nickel ions from the implants due to corrosion and wear [5]. The functional characteristics of engineering and medicinal materials are also significantly influenced by

the surface roughness at the nanoscale [6]. As a result, a nickel-free stainless steel with nanofinishing is the subject of the current effort.

It is always challenging to produce and regulate fine finishing of complicated surfaces and complex shapes. A magnetically stiffened slug of magnetorheological abrasive (MRA) fluid is extruded back and forth through and across the workpiece fixture in the MRAFF process. Metal removal from the peaks occurs only where the magnetic field is applied over the workpiece's surface, leaving all other locations untouched [7]. As it enters and exits the finishing zone, the rheological behaviour of polishing fluid moves from almost Newtonian to Bingham plastic, and vice versa. The surface of the workpiece is rubbed, and the peaks are sheared by the abrasive (cutting edges), which is supported by the chains of ferrous particles. The amount of material sheared by abrasive grains from workpiece surface peaks is determined by the strength of the MR-polishing fluid's field-induced structure [8]. Magnetorheological finishing (MRF) [9], magnetic float polishing (MFP) [10], magnetic abrasive finishing (MAF) [11], and AFM [12] are advanced fine finishing processes that aim to control the abrading forces. Although the magnetic field is used to modulate the abrading forces in MAF, MRF, and MFP, their applications are limited [13].

To preserve the versatility of MRF and AFM procedures, a new hybrid approach known as "magneto rheological abrasive flow finishing (MRAFF)" was developed [8]. This method is based on smart magnetorheological fluids, the rheological behaviour of which can be altered by an external magnetic field. According to the literature, some researchers have combined GRA and PCA to solve issues involving multiple objectives [14]. The effects of current, cycle count, and hydraulic pressure, which are anticipated to play a key role in improving surface roughness and MRR, have been studied and optimised in this work with the aid of Taguchi's L27 orthogonal array technique and the combined GRA-PCA method for effectively harnessing the MRAFF process.

2. Materials and Methods

Nickel-free austenitic stainless steel used in this study has the following chemical compositions: Cr-17%;Mn-10%;Mo-3%; Si-0.4%; C-0.5%; N-0.2%, and the remaining is Fe. There are various parts in the MRAFF setup that are shown in Figure 1. In this setup, the hydraulic cylinder is selected as a double acting cylinder with tie rod construction based on the requirements. Since the operating pressure of the cylinders will be in the range of 30 to 80 bar, a tie rod and flange mounting combination was preferred for mounting.

The rod diameter of the hydraulic cylinder is 36 mm. A piston which fits this rod was machined from a mild steel block. The outer surface of the piston was machined in such a way to accommodate the hydraulic seal. This seal prevents the seepage of magnetorheological polishing fluid (MRPF) when there is a relative movement in the container.

The fluid is pressurised by a piston that is attached to the container, which then extrudes it into the fixture for the workpiece. Here, the pressured MRPF fluid is allowed to travel through the cylindrical or flat workpiece through the workpiece fixture [15]. The fixture design is customised according to the geometry of the workpieces to be machined. Stainless steel was chosen for the fabrication of the fixture since it is nonmagnetic.

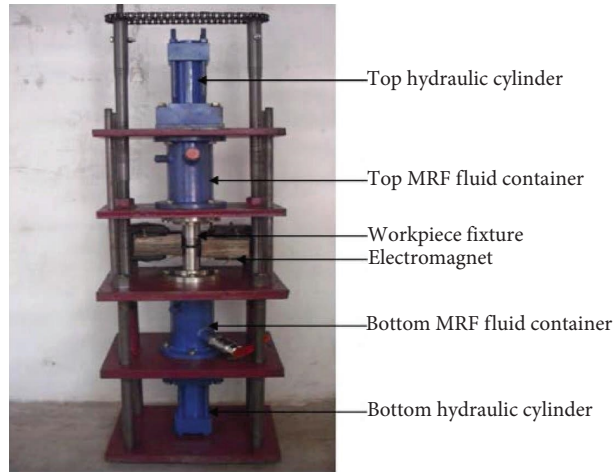

Figure 1: MRAFF experimental setup.

The electromagnet is designed to achieve a maximum magnetic flux density of 0.5 T across the workpiece in a gap of 50 mm. To avoid a greater magnetic field gradient at the corners, the core diameter is chosen to be greater than the length of the workpiece. The magnetic coil has 1530 turns, a maximum current of 10 A, a copper wire gauge of 17 SWG, a coil diameter of 103 mm with a core diameter of 50 mm, a core length of 70 mm, and steel for the core [8].

Cerium oxide and ferrous particles were selected as constituents of MRA fluid in the following ratios: 60% of the volume is silicone oil base fluid, 20% is cerium oxide (300 mesh size), and 20% is ferrous particle (400 mesh size). Figure 2 shows the morphologies of ferrous and cerium oxide particles captured by a scanning electron microscope (SEM), and it is observed that for the identical scale, the ferrous particles are bigger than cerium oxide particles. It also demonstrates that ferrous particles are with curvy round edges in the periphery, but the cerium oxide particles are existing with sharp edges which are required to conduct the metal removal process.

Oleic acid, a surfactant was introduced together with cerium oxide and ferrous particles to keep the particles in Brownian motion. The mechanical stirrer was used to stir the mixture. The stirring lasts for thirty minutes. With the aid of a mechanical stirrer, this liquid is then once again combined with silicone oil and AP3 grease. A C-shaped electromagnet is encompassing the workpiece fixture in such a way that magnetic lines are perpendicular to the workpiece surface kept in the fixture.

The workpiece fixture held 50 SS 316L workpieces measuring $50 \times 10 \times 4$ mm and having an initial SR of 0.18 μm. Before the MRAFF process begins, the MRA fluid is loaded into the experimental setup, the required pressure is set in the hydraulic power pack, and the voltage in the

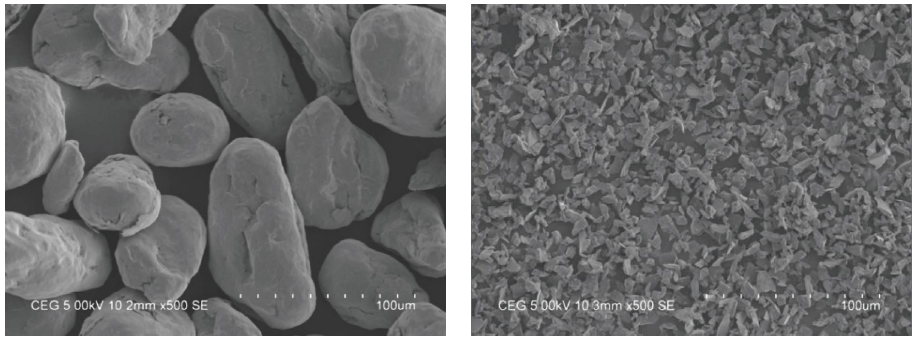

(a) (b)

Figure 2: SEM images of (a) Fe particles (b) CeO_2 particles.

electromagnet is set using a regulated power supply. The rheological nature of the MRA fluid is precisely controlled by the magnetic flux density produced by the electromagnet, which is directly proportional to the supply voltage. The Fe particles in the MRA fluid inside the workpiece fixture will be scattered in the absence of a magnetic field. When the electromagnet is turned on, the Fe particles in the MRA fluid form chains, and the strength of the chains increases.

A method for consecutive operation of hydraulic cylinders at an appropriate pressure reacts to the Fe chains and CeO_2 particles. The scraping power produced and metal expulsion from the workpiece are dependent on the firmness of the ferrous chains, abrasive particles held by them, and hydraulic pressure [16], which can produce a surface finish at the nanometer level on even difficult to machine materials.

2.1. Design of Experiments-Taguchi Technique. The L27 series was chosen to optimise these process parameters using the Taguchi approach due to the effects of the MRAFF's extrusion pressure, current, and number of cycles (NOC) on the surface roughness of the stainless-steel workpiece. Table 1 displays the selected input parameters and their levels.

Dr. Genichi Taguchi's theory in quality building is that quality must be built into the item and be insensitive to noise causes by reducing the deviation of qualities from goal qualities and execution of things [17]. He was able to separate the contour of orthogonal displays from the concept of graphical linear connection. Taguchi advised the use of additive models and linear graphs.

In the case of an additive model, the primary effects alone are examined, and the effects of interactions are ignored, but the linear graph displays information about the interactions. Taguchi employs the signal-to-noise (S/N) ratio, which connects mean with variance. The proportion S/N is determined by the kind of value attributes, with greater being better, smaller being better, and nominal being better. The greater the better option was applied for MRR and smaller the better was preferred for surface roughness in this experimental work, which is referred by:

$$\frac{S}{N} = -10 \log \left(\frac{1}{n} \sum_{i=1}^{n} \frac{1}{y_i^2} \right). \tag{1}$$

Table 1: Factors and their levels.

Parameters	Level 1	Level 2	Level 3
Pressure (bar)	20	30	40
Current (A)	2	4	6
No of cycles	100	200	300

The idea of smaller the better is given by:

$$\frac{S}{N} = -10 \log \left(\frac{1}{n} \sum_{i=1}^{n} y_i^2 \right). \tag{2}$$

2.2. Grey Relational Analysis. In some real-time situations, the information imagined by the data may not be completely black and white (i.e., no information or full information). The outcomes of these challenges may be fuzzy or cloudy and are sometimes referred to as grey. Grey relational analysis (GRA) refers to an analysis that includes uncertain and partially understood factors. The initial phase of GRA is data preprocessing, where normalised values are used. The original sequence is normalised here, while the processed data sequence is supplied by

$$x_i^*(k) = \frac{x_i^0(k) - \min x_i^0(k)}{\max x_i^0(k) - \min x_i^0(k)}. \tag{3}$$

The original data sequence is given by $x_i^0(k)$ in the aforementioned equation, while the biggest and smallest values are denoted by $\max x_i^0(k)$ and $\min x_i^0(k)$, respectively. The reference sequence is found when scaling the performance sequence is in between 0 and 1 using the normalisation process. When the data value is near to 1, it is chosen as the best response since it contains the most needed information. For the purpose of correlating the idea as well as experimental responses, the grey relational coefficient is calculated as

$$\zeta(k) = \frac{\Delta_{\min} + \zeta.\Delta_{\max}}{\Delta_{0i}(k) + \zeta.\Delta_{\max}}, \tag{4}$$

where $\Delta_{0i}(k)$ is the deviation sequence given by

$$\Delta_{0i}(k) = \left\| x_0^*(k) - x_i^*(k) \right\|,$$
$$\Delta_{\max} = \max_{\forall j \in i} \max_{\forall k} \left\| x_0^*(k) - x_j^*(k) \right\|, \quad (5)$$
$$\Delta_{\min} = \min_{\forall j \in i} \min_{\forall k} \left\| x_0^*(k) - x_j^*(k) \right\|.$$

Here, ζ is known as identification coefficient, $\zeta \in [0, 1]$ and normally $\zeta = 0.5$ is used. The grey relational grade is calculated by taking the average of all grey relational coefficients of output responses, and it is given by

$$\gamma_i = \frac{1}{n} \sum_{k=1}^{n} i\zeta_i(k). \quad (6)$$

2.3. Principal Component Analysis. For a set of variables in the existence of systematic interdependence, a multivariate technique applied was referred as factor analysis. Principal component analysis (PCA) is a type of multivariate strategy in which all the information about the real variables are consolidated by a mathematical technique by means of either lesser or uncorrelated set of combinations with minimum loss of information [18]. The PCA consolidates factors representing largest variances to build up the main key part and the following largest variable meant for the consequent principal component, until the sample variances are accumulated as component groups.

PCA is used to address issues based on multiobjective optimisation utilising Taguchi's approach. The PCA is a method for elucidating various covariance patterns using a direct mix of measured properties. The PCA strategy [19] used in this work consists of the following steps:

Step 1: Development of characteristic array of multiple responses

$$\begin{pmatrix} x_1(1) & x_1(2) & \dots & \dots & x_1(n) \\ x_2(1) & x_2(2) & \dots & \dots & x_2(n) \\ \vdots & . & \dots & \dots & \vdots \\ \vdots & . & \dots & \dots & \vdots \\ x_m(1) & x_m(2) & \dots & \dots & x_m(n) \end{pmatrix}, \quad (7)$$

where $x_i(j)$ denotes the value in the matrix, $i = 1, 2, 3, \dots, m$; $j = 1, 2, 3, \dots, n$. In this study, X is the normalised S/N ratio of each response and $m = 27$, $n = 3$.

Step 2: Generation of the correlation coefficient array

It is generated as:

$$R_{jl} = \left(\frac{\mathrm{Cov}(x_i(j), x_i(l))}{\sigma_{Xi}(j) X \sigma_{Xi}(l)} \right), \; j = 1, 2, 3 \dots n; l. \quad (8)$$

Here, the sequence covariance of x_i (j) and x_i (l) is referred as Cov (x_i (j) and x_i (l)): standard deviation of $x_i(j)$ is denoted *as* σ_{xi} (j); and standard deviation of $x_i(l)$ sequence is referred as r σ_{xi} (l).

Step 3: Calculation of Eigen vectors and values

Eigenvectors and values are calculated by using the correlation array.

$$(R - \lambda_k I_m) V_{ik} = 0, \quad (9)$$

where λ_k refers to the eigen values $\sum_{k=1}^{n} \lambda_k = n, k = 1, 2, 3 \dots n$; $V_{ik} = [a_{k1} a_{k2} \dots a_{kn}]^T$ refers to the eigen vectors for the respective eigen value λ_k.

Step 4: Determination of the principal components

The formulation of the uncorrelated principal components is formulated as follows:

$$Y_{mk} = \sum_{i=1}^{n} X_m(i) \cdot V_{ik}, \quad (10)$$

where Y_{m1} and Y_{m2} are the first and second principal components and so on. Based on variance, the principal components are arranged in decreasing order with respect to the variance and many of the variances in the data are related to the first principal component.

3. Results and Discussion

Optimization software Minitab 16.0 was used to formulate L27 experiments in order to optimise the process parameters of the Magnetorheological abrasive flow finishing process by the Taguchi method.

3.1. Surface Measurements and MRR. The stainless-steel workpieces machined by the MRAFF process were analysed by Talysurf Coherence Correlation Interferometer (CCI). By considering the mass of the workpiece before and after the machining and machining time, MRR for each sample was calculated.

The surface roughness of the stainless-steel workpieces were measured by Talysurf Coherence Correlation Interferometer (CCI). The 3D surface of the workpiece along with the 2D graph is shown in Figure 3. During the measurement, the focused area was kept as $3\,\mu\mathrm{m} \times 3\,\mu\mathrm{m}$, the evolution length was 0.8 mm, and the vertical resolution was 0.01 nm (0.1 A°). More surface irregularities could be observed on the SS 316L sample before the MRAFF process and a smaller number on the sample after the MRAFF process from the 3D profiles. In each sample, three surface measurements were made at different locations and their mean values have been used for the study.

3.2. Combined GRA-PCA. For the purpose of normalising the outputs, equation (1) is used. In GRA, normalising is followed by deviation sequence. After the calculation of deviation sequence, the grey relational coefficients were found by using equation (2). Principle component analysis was used to find MRPI [20], and all the aforementioned values are given in Table 2.

From the experimental results by considering the mean value of the responses, it is observed that when the hydraulic pressure is increased from 30 to 40 bar, MRR was reduced by 10.13%, and SR was increased by 1.35%. While the hydraulic

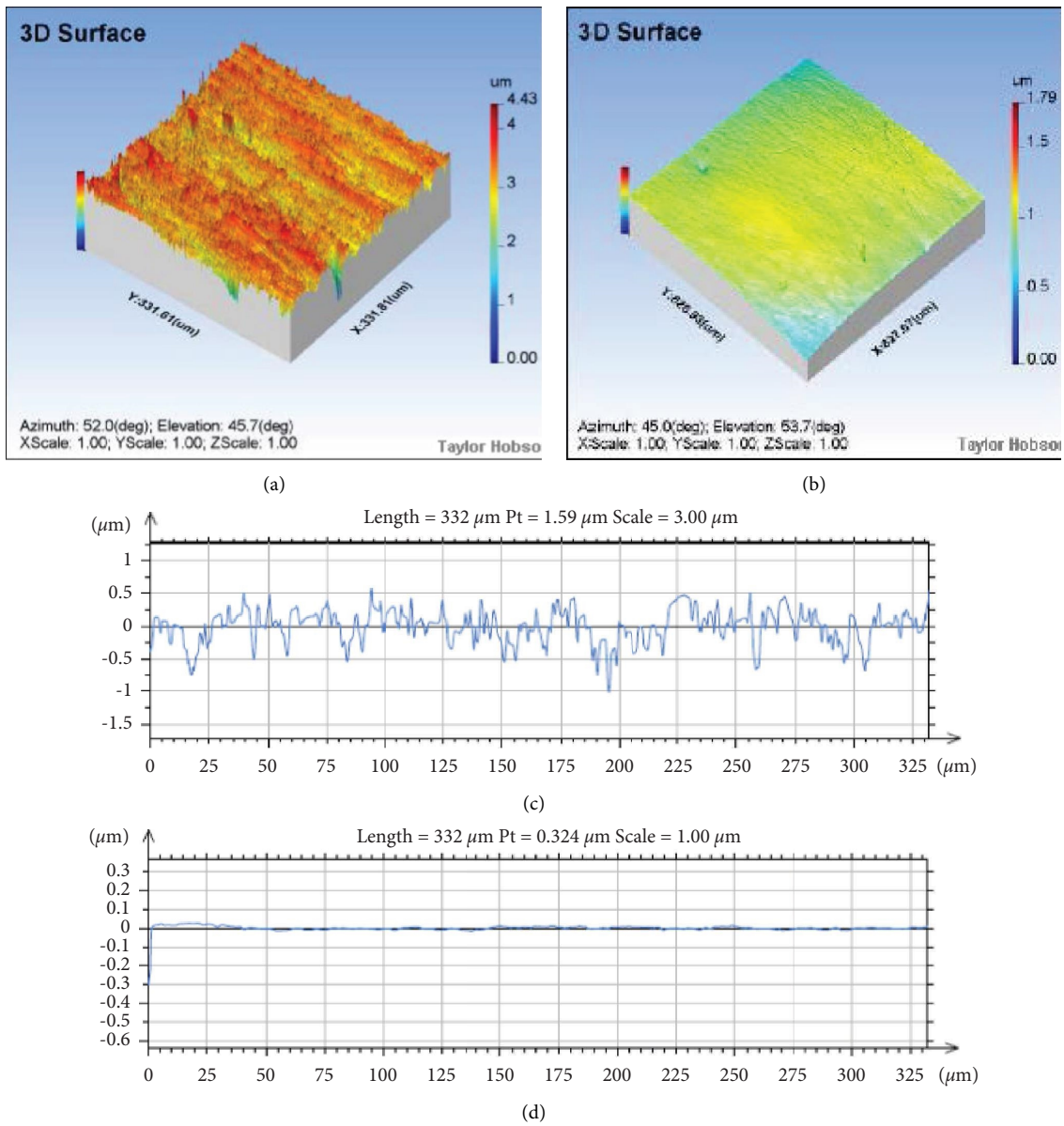

Figure 3: 3D surface of SS 316L (a) before MRAFF process, (b) after MRAFF process 2D graph of SS 316L surface, (c) before MRAFF process and, (d) after MRAFF process.

pressure is increased from 40 to 50 bar, an increment of 1.37% of MRR and 2.07% of SR were observed.

When the supply current to the electromagnet is increased from 2 to 4 A, 78.26% increment in MRR and 10.32% reduction of SR were observed. The further increase in current from 4 to 6 A increases the MRR by 48.09% and reduces the SR by 10.27%. The increase in NOC from 100 to 200 leads to increase the MRR by 32.1% and decrease the SR by 5.27%. The subsequent increase of NOC from 200 to 300 reduces the SR by 5.08% and increases the MRR by 30.75%.

From the results of PCA, the selected given vectors for MRR and SR are 0.707 and 0.707 since the Eigen value is 1.9276 which is greater than 1 and desirable as given in Table 3. The average value of MRPI [21] for the selected levels of input parameters, the optimal values are found and given in Table 4. The pressure of 30 bar, current of 6 A, and 300 number of cycles were found as optimum levels.

The variations of Multiresponse Performance Index (MRPI) for all the levels of input parameters are shown as the main effect plot in Figure 4. In this graph, the pressure values are 30, 40, and 50 bar at the level 1, 2, and 3, respectively. Similarly, current values are 2, 4, 6 A and number of cycles are 100, 200, and 300, respectively, at three levels.

Biplots are a type of statistical exploratory graph that is a generalisation of the two-variable scatterplot. A biplot is a combination of a score plot and loading plot. The biplot is a graphical representation of information from both samples and variables in a data matrix. Vectors, linear axes, and nonlinear trajectories are used to represent variables, while points are used to represent samples. In the case of

Table 2: Results of Taguchi's L27-series of experiments.

Trial no	Input control parameters			Output responses		Normalising sequence		Deviation sequence		Grey relational coefficient		Principal components		Multiresponse performance index (MRPI)
	Pressure (bar)	Current (A)	NOC	MRR (mg/sec)	R_a (nm)	MRR (mg/sec)	R_a (nm)	MRR (mg/sec)	R_a (nm)	MRR (mg/sec)	R_a (nm)	MRR (mg/sec)	R_a (nm)	
1	30	2	100	0.448	83.35	0.104	0.021	0.896	0.979	0.358	0.338	0.179	0.169	0.174
2	30	2	200	0.831	78.25	0.285	0.215	0.715	0.785	0.411	0.389	0.206	0.194	0.200
3	30	2	300	1.161	74.63	0.441	0.352	0.559	0.648	0.472	0.435	0.236	0.218	0.227
4	30	4	100	1.158	73.76	0.439	0.385	0.561	0.615	0.471	0.448	0.236	0.224	0.230
5	30	4	200	1.39	69.93	0.549	0.530	0.451	0.470	0.526	0.515	0.263	0.258	0.260
6	30	4	300	1.788	66.08	0.736	0.676	0.264	0.324	0.655	0.607	0.327	0.303	0.315
7	30	6	100	1.815	66.23	0.749	0.670	0.251	0.330	0.666	0.603	0.333	0.301	0.317
8	30	6	200	2.147	63.16	0.906	0.787	0.094	0.213	0.841	0.701	0.421	0.350	0.385
9	30	6	300	2.312	57.53	0.983	1.000	0.017	0.000	0.968	1.000	0.484	0.500	0.492
10	40	2	300	1.053	74.92	0.390	0.341	0.610	0.659	0.450	0.431	0.225	0.216	0.220
11	40	2	100	0.227	82.64	0.000	0.048	1.000	0.952	0.333	0.344	0.167	0.172	0.169
12	40	2	200	0.647	78.78	0.198	0.194	0.802	0.806	0.384	0.383	0.192	0.191	0.192
13	40	4	300	1.712	67.36	0.700	0.627	0.300	0.373	0.625	0.573	0.313	0.286	0.299
14	40	4	100	1.052	75.87	0.389	0.305	0.611	0.695	0.450	0.418	0.225	0.209	0.217
15	40	4	200	1.213	71.24	0.465	0.480	0.535	0.520	0.483	0.490	0.241	0.245	0.243
16	40	6	300	2.112	59.80	0.889	0.914	0.111	0.086	0.819	0.853	0.409	0.426	0.418
17	40	6	100	1.675	66.76	0.683	0.650	0.317	0.350	0.612	0.588	0.306	0.294	0.300
18	40	6	200	2.037	64.12	0.854	0.750	0.146	0.250	0.774	0.667	0.387	0.333	0.360
19	50	2	200	0.621	79.02	0.186	0.185	0.814	0.815	0.380	0.380	0.190	0.190	0.190
20	50	2	300	1.508	78.55	0.604	0.203	0.396	0.797	0.558	0.386	0.279	0.193	0.236
21	50	2	100	0.266	83.91	0.018	0.000	0.982	1.000	0.337	0.333	0.169	0.167	0.168
22	50	4	200	1.275	72.51	0.494	0.432	0.506	0.568	0.497	0.468	0.249	0.234	0.241
23	50	4	300	1.654	67.28	0.673	0.630	0.327	0.370	0.605	0.575	0.302	0.287	0.295
24	50	4	100	0.812	76.38	0.276	0.285	0.724	0.715	0.408	0.412	0.204	0.206	0.205
25	50	6	200	1.804	64.97	0.744	0.718	0.256	0.282	0.661	0.639	0.331	0.320	0.325
26	50	6	300	2.347	63.24	1.000	0.784	0.000	0.216	1.000	0.698	0.500	0.349	0.424
27	50	6	100	1.602	68.85	0.649	0.571	0.351	0.429	0.587	0.538	0.294	0.269	0.281

Table 3: Eigen values and variation of principal components.

Components	Eigen value	Difference	Variation (%)	Cumulative (%)	Eigenvector [MRR and SR]
Z1 component	1.9276	0.700	96.40	96.40	[0.707, 0.707]
Z2 component	0.0724	0.667	3.60	100.00	[0.707, −0.707]

Table 4: Response table for grey relational grade.

Factors	Level 1	Level 2	Level 3	Max–Min
Pressure	0.289	0.269	0.263	0.026
Current	0.197	0.256	0.367	0.170
NOC	0.229	0.266	0.325	0.096

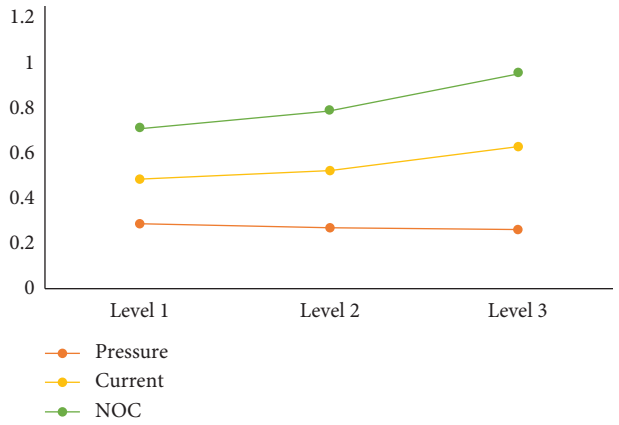

Figure 4: Main effect plot for MRPI variation.

categorical variables, category level points can be used to represent the levels of a categorical variable. A generalised biplot shows data on both continuous and categorical variables. The biplot as shown in Figure 5 is used to interpret the overall scoring of Eigen values with respect to the responses simultaneously. It is utilised to describe the location of one response over the other by means of the principal components. Biplot depicts the available subspace along with the score points. For the initial two parts, biplot finds the proportion between the perceptions and factors accessible in subspace.

In PCA, the loading plot is used to determine which variables have the greatest impact on each component. Loadings can range from −1 to 1. Loadings close to −1 or 1 indicate that the variable has a significant impact on the component. Loadings close to zero indicate that the variable has little effect on the component. The loading plot can help you figure out which variables have the most influence on each component. Loadings can range from −1 to 1. Loadings close to −1 or 1 indicate that the variable has a significant impact on the component. Loadings close to zero indicate that the variable has little effect on the component. The loading plot in Figure 6 shows that when primary segment 1 and vital segment 2 expand, the estimation of MRR increases while the assessment of surface roughness decreases, indicating a link between these two yield responses.

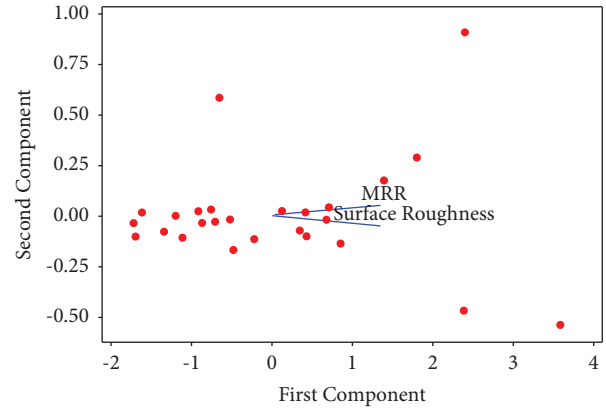

Figure 5: Biplot for MRR and SR.

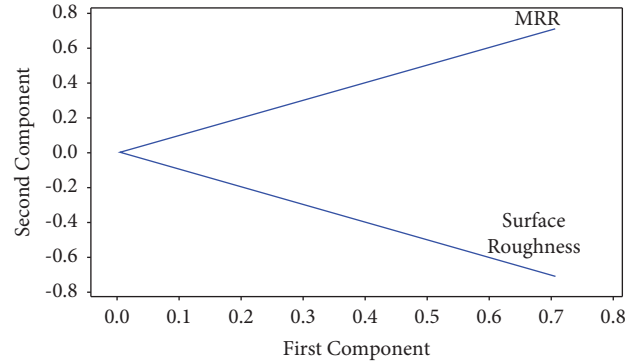

Figure 6: Loading plot for MRR and SR.

From the interaction plot for MRPI as shown in Figure 7, it is observed that the interaction is existing in between hydraulic pressure and current as well as hydraulic pressure and number of cycles since all other combinations are showing the MRPI variations without any interactions.

Analysis of variance (ANOVA) as given in Table 5 is utilised to summarise the percentage contribution of input parameters on the output response [22]. From this table, it is understood that the current to the electromagnet is the most dominant input parameter; it holds 70.74% contribution followed by the number of cycles and hydraulic pressure each of them having 22.41% and 1.78% contribution, respectively.

3.3. Effect of Hydraulic Pressure. When the hydraulic extrusion pressure is increased from 30 to 50 bar, the surface roughness and MRR on stainless-steel workpieces depict that there is no appreciable improvement because of the increase in hydraulic pressure [23]. Since the pressure values

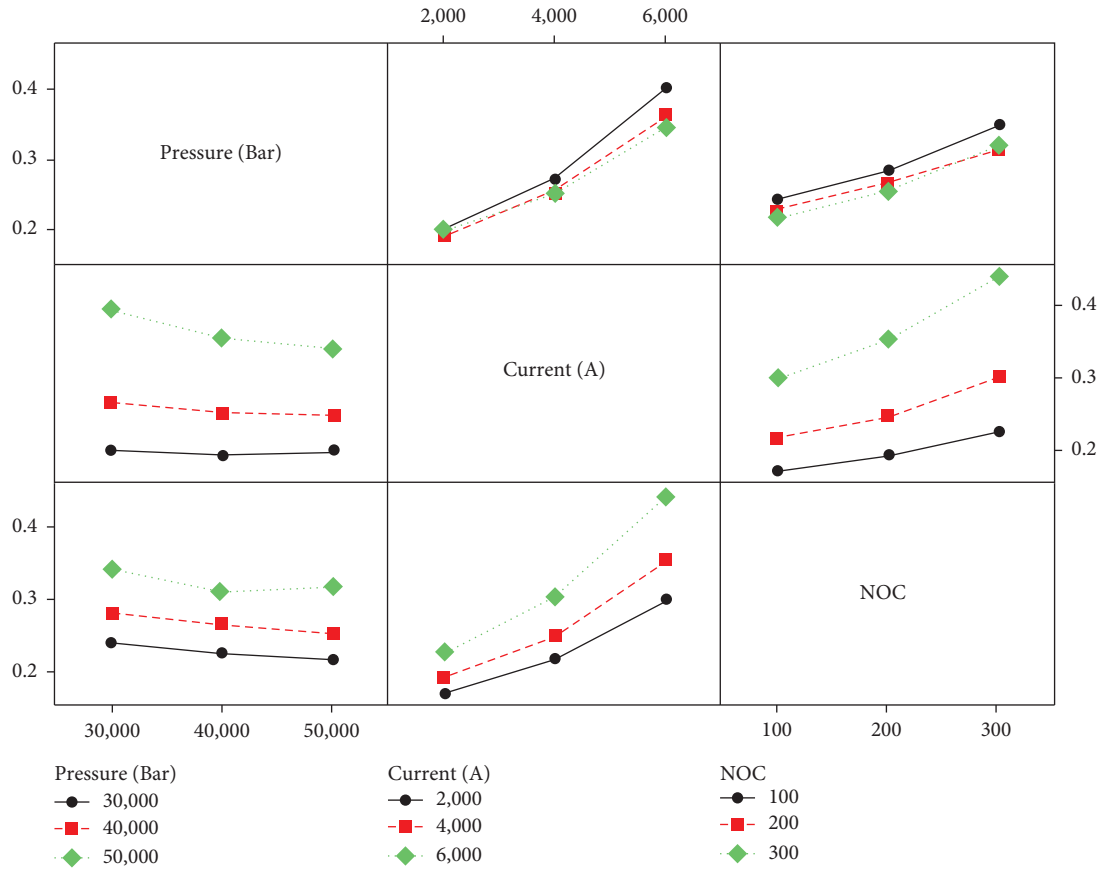

Figure 7: Interaction plot for mean MRPI.

Table 5: Analysis of variance.

Source	DF	SeqSS	Adj SS	Adj MS	*F*	*P*	% Count
Pressure (bar)	2	0.0034	0.0034	0.0017	3.52	0.05	1.78
Current (A)	2	0.1335	0.1335	0.0668	139.5	≤0.001	70.7
NOC	2	0.0422	0.0423	0.0212	44.22	≤0.001	22.4
Error	20	0.0096	0.0095	0.0005			5.06
Total	26	0.1888					

$S = 0.0218703$ R-Sq = 94.93% R-Sq (adj) = 93.41%.

used does not induce much on the indentation/shearing force on the ferrous chains as well as abrasive particles, no significant correlation is obtained for hydraulic pressure on output responses.

3.4. Effect of Current. As the current is raised from 2 A to 6 A, the surface roughness of stainless-steel workpieces continues to diminish, and the surface quality improves. The surrounding ferrous chains boost the bonding strength of the abrasive particles as a result of the greater magnetic flux density caused by the rise in current [23]. As a result, the abrasive particles' inclination to spin is considerably decreased, and they are actively involved in material removal and lowering surface roughness.

3.5. Effect of Number of Cycles. The surface smoothness improved significantly when the number of cycles was increased from 100 to 300 [24]. The removal of loosely held material left over after the surface grinding was primarily responsible for the first reduction in surface roughness. The deeper grinding marks are removed after the entire material burrs have been removed, further reducing surface roughness.

3.6. Validation of Optimised Results. Validation experiments were carried out to validate the optimised GRA-PCA results, which are shown in Table 6. Validation results are found to deviate from predicted values by no more than 5%. As a result, the model developed using the response surface

Table 6: Validation of optimised results.

Optimised input process variables			Validation experiments	Responses			
Pressure (bar)	Current (A)	NOC		SR (nm)	% difference	MRR (mg/sec)	% difference
30	6	300	1	62.28	−1.52	2.28	−2.56
			2	63.29	0.08	2.36	0.85
			3	62.28	−1.52	2.29	−2.14
			4	61.14	−3.32	2.34	−0.00
			5	63.18	−0.09	2.33	−0.43

methodology can be used to predict the final Ra and MRR of nickel-free austenitic stainless-steel within the range of input variables chosen.

4. Conclusion

Experiments were carried out to study the effects of current, cycle count, and extrusion pressure on the surface finish in order to optimise the MRAFF process parameters and obtain a nano level surface finish on nickel-free stainless-steel workpieces. The findings below are the result of the experimental study. Minitab 16.0 software was used to optimise the process parameters.

(i) With respect to the experimental results and analysis carried out, the increase in hydraulic pressure plays a least significant role towards the responses

(ii) The most dominant input parameter is the current to the electromagnet as it plays a major role in the amount of metal removal from the workpiece surface that tends to achieve surface roughness at the nano level

(iii) When compared with the other two input parameters, a moderate role is played by the number of cycles towards the final SR and MRR

(iv) From the GRA-PCA technique, the optimum combination of input parameters that results in minimum SR along with maximum MRR is identified as 30 bar pressure, 6 A current, and 300 number of cycles

Data Availability

The data used to support the findings of this study are available from the corresponding author upon request.

Conflicts of Interest

The authors declare that they have no conflicts of interest.

References

[1] A. La Monaca, J. W. Murray, Z. Liao et al., "Surface integrity in metal machining-Part II: functional performance," *International Journal of Machine Tools and Manufacture*, vol. 164, Article ID 103718, 2021.

[2] C. Sheng, H. Zhu, and L. Li, "Hybrid vibration control using magnetorheological dampers and elastomers for civil structural," *AIP Advances*, vol. 12, no. 2, Article ID 025222, 2022.

[3] S. Krishnakumar and K. Manivannan, "Retracted article: effective segmentation and classification of brain tumor using rough K means algorithm and multi kernel SVM in MR images," *Journal of Ambient Intelligence and Humanized Computing*, vol. 12, no. 6, pp. 6751–6760, 2021.

[4] P. Dong, T. Zhang, H. Xiang et al., "Controllable synthesis of exceptionally small-sized superparamagnetic magnetite nanoparticles for ultrasensitive MR imaging and angiography," *Journal of Materials Chemistry B*, vol. 9, no. 4, pp. 958–968, 2021.

[5] K. Yang and Y. Ren, "Nickel-free austenitic stainless steels for medical applications," *Science and Technology of Advanced Materials*, vol. 11, no. 1, Article ID 014105, 2010.

[6] S. Kathiresan and B. Mohan, "Multi-objective optimization of magneto rheological abrasive flow nano finishing process on AISI stainless steel 316L," *Journal of Nano Research*, vol. 63, pp. 98–111, 2020.

[7] W. Zhang, "Polishing and MagneticField–assisted finishing," *Intelligent Energy Field Manufacturing*, CRC Press, pp. 579–594, 2018.

[8] S. Jha and V. K. Jain, "Design and development of the magnetorheological abrasive flow finishing (MRAFF) process," *International Journal of Machine Tools and Manufacture*, vol. 44, no. 10, pp. 1019–1029, 2004.

[9] W. Kordonski and D. Golini, "Progress update in magnetorheological finishing," *International Journal of Modern Physics B*, vol. 13, no. 14n16, pp. 2205–2212, 1999.

[10] Y. Tani, K. Kawata, and K. Nakayama, "Development of high-efficient fine finishing process using magnetic fluid," *CIRP Annals*, vol. 33, no. 1, pp. 217–220, 1984.

[11] T. Shinmura, K. Takazawa, E. Hatano, M. Matsunaga, and T. Matsuo, "Study on magnetic abrasive finishing," *CIRP annals*, vol. 39, no. 1, pp. 325–328, 1990.

[12] L. J. Rhoads, "Abrasive flow machining," *Journal of Materials Processing Technology*, vol. 28, pp. 75–78, 1991.

[13] S. Kathiresan, K. Hariharan, and B. Mohan, "Prediction of surface roughness in magneto rheological abrasive flow finishing process by artificial neural networks and regression analysis," *Applied Mechanics and Materials*, vol. 706, 2015.

[14] N. Senthilkumar, V. Selvakumar, and T. Tamizharasan, "Optimization and performance analysis of uncoated and coated carbide inserts during hard turning AISI D2 steel using hybrid GRA-PCA technique," *Applied Mechanics and Materials*, vol. 852, pp. 151–159, 2016.

[15] M. B. KathiresanSundararaj, "Vitro biocompatibility study on stainless steel 316l after nano finishing," *Biomedical and Biotechnology Engineering*, vol. 58363, 2017.

[16] Z. Alam, F. Iqbal, and S. Jha, *Modeling and Analysis of Forces and Finishing Spot Size in the ball End Magnetorheological Finishing (BEMRF) Process*, Elsevier, Amsterdam, Netherlands, 2022.

[17] P. Chandramohan, S. N. Murugesan, and S. Arivazhagan, "Heat transfer analysis of flat plate subjected to multi-jet air

impingement using principal component analysis and computational technique," *Journal of Applied Fluid Mechanics*, vol. 10, no. 1, pp. 293–306, 2017.

[18] H. Hotelling, "Analysis of a complex of statistical variables into principal components," *Journal of Educational Psychology*, vol. 24, no. 6, pp. 417–441, 1933.

[19] H.-C. Liao, "Multi-response optimization using weighted principal component," *International Journal of Advanced Manufacturing Technology*, vol. 27, no. 7-8, pp. 720–725, 2006.

[20] A. M. ErgünEkici and U. Gültekin, "Multi-objective optimization of process parameters for drilling fibermetal laminate using a hybrid gra-pca approach," *FME Transactions*, vol. 49, 2021.

[21] S. Thirumalvalavan, N. Senthilkumar, G. Perumal, and M. R. AnanthaPadmanaban, "Ameliorating the wear defiance of hvof thermal spray silicon carbide coated ti-6al-4v alloy using pca-gra technique," *Silicon*, vol. 14, 2022.

[22] M. Kumar, S. Ahmad, and M. Das, "Magnetorheological-finishing of miniature gear teeth profiles using uniform flow restrictor," *Materials and Manufacturing Processes*, vol. 37, 2021.

[23] S. Jha, V. K. Jain, and R. Komanduri, "Effect of extrusion pressure and number of finishing cycles on surface roughness in magnetorheological abrasive flow finishing (MRAFF) process," *International Journal of Advanced Manufacturing Technology*, vol. 33, no. 7-8, pp. 725–729, 2006.

[24] K. Arora and A. K. Singh, "Magnetorheological finishing process for improved performance of polymer gears," *Materials and Manufacturing Processes*, 2021.